Nature of ferroelectric-paraelectric phase transition and origin of negative thermal expansion in $PbTiO_3$

Huazhi Fang,* Yi Wang, Shunli Shang, and Zi-Kui Liu
Department of Materials Science and Engineering, The Pennsylvania State University, University Park, Pennsylvania 16802, USA
(Received 5 August 2014; revised manuscript received 16 December 2014; published 9 January 2015)

Ferroelectric-paraelectric (FE-PE) phase transitions have been primarily explained by the phenomenological Landau-Devonshire theory and a soft-zone-center mode of vibration in the literature. In this work, we study the atomic structure and polarization evolution of $PbTiO_3$ as a function of temperature using *ab initio* molecular dynamics simulations. In contrast to conventional molecular dynamics analyses where results are averaged over time, we categorize the atomic configurations as a function of time in terms of Ti-O bond lengths in the nearest-neighboring shell. We show that an appreciable amount of cubic configuration exists at temperatures about 300 K below its FE-PE phase transition temperature of 763 K, even though the time-averaged overall atomic configuration is tetragonal. The quantitative results depict that as the temperature increases the population of the cubic configuration increases and that of the tetragonal configuration decreases, signifying that the FE-PE phase transition is intrinsically second order. It reveals that the thermal fluctuation of the cubic configurations in the tetragonal matrix makes a significant contribution to the negative thermal expansion in the FE phase region because the cubic configuration has smaller volume and higher entropy than the tetragonal matrix.

DOI: 10.1103/PhysRevB.91.024104 PACS number(s): 77.80.B−, 31.15.A−, 31.15.xv

I. INTRODUCTION

Ferroelectric materials directly convert electrical energy to mechanical energy and are critical to applications such as sensors, transducers, actuators, and cooling devices. Perovskite $PbTiO_3$ is one of the most extensively studied ferroelectric materials [1]. In $PbTiO_3$, two atomic configurations have been known for a long time, i.e., ferroelectric tetragonal (FE) and paraelectric cubic (PE) [2], until rather recently when several other structures were reported at high pressures [3,4]. $PbTiO_3$ shows the FE to PE phase transition at about 763 K at ambient pressure and at room temperature at about 12 GPa [1,5–9]. The FE phase has a large tetragonal distortion with an axis ratio of $c/a = 1.06$ at room temperature, resulting in considerably large spontaneous polarization and ionic shifts, high Curie temperature T_c, and a wide temperature region in which the tetragonal phase is stable along with the negative thermal expansion (NTE) phenomenon [1,5,7]. Although the $PbTiO_3$ is of a model ferroelectric perovskite discovered 60 years ago, the nature of the FE-PE phase transition mechanism and the origin of NTE still remain controversial. It has been generally accepted that the FE-PE transition is first order under ambient pressure [10,11]. However, through detailed analysis of pressure-volume relations and temperature-volume phase diagrams reported in the literature, we recently showed that the FE-PE transition of $PbTiO_3$ in the temperature and pressure ranges studied is second order instead under zero external electric field [2]. While the FE-PE phase transition is regarded as the typical displacive one associated with softening of the relevant phonon modes, a certain degree of order-disorder mechanism has been considered in the literature [12–16] associated with the orientation change of local distortions. Sicron *et al.* [12–14] studied the local atomic distortion of $PbTiO_3$ crystal using the x-ray absorption fine-structure structure (XAFS) technique which is able to provide quantitative structural information on the atomic scale within a very short effective measuring time on the order of 10^{-16} s. They found that Pb and Ti atoms are displaced from the ideal structures both below and above the phase transition temperature and locally unit cells remain tetragonal even well above the transition temperature. Similar results were found by Miyanaga *et al.* [15] and Sato *et al.* [16] through measuring the Pb-edge and the Ti-edge XAFS spectra, respectively.

Previous theoretical studies mostly focus on the lattice dynamics and electronic band structure of the ferroelectric pervoskite using density functional theory, and only a few studies are conducted for exploring structural evolution and phase transition at finite temperatures. Since the tetragonal to cubic phase transition is mainly displacive instead of diffusive [17–19], it is feasible to study the solid-state phase transition in $PbTiO_3$ within the time scale (100 ps–10 ns) that molecular dynamics simulations can presently reach. Srinivasan *et al.* [20] studied temperature-induced FE-PE transition in $PbTiO_3$ through *ab initio* molecular dynamics (AIMD) simulations. However, they did not look into the details of atomic configurations and spontaneous polarization and overestimated the phase transition temperature as 944 K at zero pressure. Costa *et al.* [21] studied both temperature- and pressure-induced structural phase transitions in $PbTiO_3$ through the classical MD method using empirical pair potentials, and reported the transition temperature was 1100 K at zero pressure and the transition pressure was 5 GPa at 100 K, considerably different from the experimental data. Recently, through a MD study based on a first-principles parametrized force field, Mani *et al.* [22] indicated the presence of order-disorder mechanism in the vicinity of the phase transition in the classic displacive $PbTiO_3$ ferroelectric. However, their simulations did not reproduce the experimental observations of local tetragonal distortions well above the phase transition temperature [12,15,16].

In this paper, we study the details of atomic configurations of $PbTiO_3$ as a function of time and temperature by the AIMD approach [23,24]. In the AIMD approach the classical mechanics is used to describe molecular dynamics with the

*huf12@psu.edu

interatomic force generated on the fly from the ground state of electrons within density functional theory. It will be shown that the statistical analysis as a function of time, instead of the conventional time averaging, is the key in probing the microscopic mechanisms of the FE-PE transition.

II. COMPUTATIONAL METHODS

The AIMD calculations in the current work are performed by employing the Vienna *ab initio* simulation package (VASP) [25,26]. The first-principles calculations presented here are based on the density functional theory with the ion-electron interaction described by the Vanderbilt ultrasoft pseudopotentials and the electronic exchange correlation by the local density approximation (LDA). The valence electrons considered in the pseudopotentials for each atomic species are as follows: $6s^2 6p^2$ for Pb, $3d^3 4s^1$ for Ti, and $2s^2 2p^4$ for O. Within the low-precision scheme, we use the Γ point only to sample the Brillouin zone and a cutoff energy of 396 eV for the plane wave basis using a supercell containing 135 atoms: i.e., 27 Pb, 27 Ti, and 81 O. The supercell lattice parameters are from the experimental data by Shirane *et al.* [1] measured by the x-ray method and the extrapolated ones for the temperatures of 900 and 1000 K due to the absence of experimental data (as shown in the Supplemental Material [27]).

The size and shape of supercells are kept fixed whereas the ions are allowed to relax during the AIMD simulations. The simulations are performed in a canonical ensemble (*NVT*) with a Nosé thermostat [28] for temperature control. The Newton's equation of motion is solved via the Verlet algorithm with a time step of 3 fs, and a total simulation time of ∼21 ps is taken so as to obtain sufficient AIMD configurations for statistical analysis. It is mentioned that even though AIMD simulation at constant pressure (*NPT*) can also be accessible in recent versions of VASP, we believe the *NVT* ensemble with the overall lattice parameters fixed to the experimental ones is more appropriate and accurate for our purpose, as we assume the overall supercell does not change while the local atomic structure fluctuates at a given temperature.

III. RESULTS AND ANALYSES

A. Structural evolution and FE-PE phase transition

Conventionally, the general structural features could be characterized through the pair correlation function (PCF) or the triplet correlation function (TCF), which of present work are in good agreement with the x-ray diffraction measurements [29,30], as shown in the Supplemental Material [27]. However, the PCF and TCF are derived through statistical average over the entire AIMD ensemble and time steps and cannot provide the specific information on instantaneous local atomic distortion and polarization. Motivated by the XAFS measurements of Sicron *et al.* [12–14], we explore the distortions of local unit cells as a function of temperature, in terms of local cell parameters and atomic displacements relative to the centrosymmetric cubic structure. The results are shown in Figs. 1 and 2 in comparison with experimental data. It can be seen that our predicted results are in good agreement with those determined from the XAFS experiments qualitatively, whereas they are significantly different from those measured

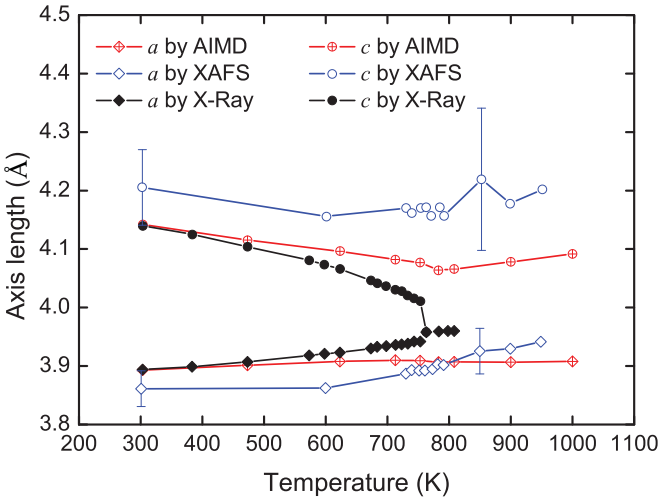

FIG. 1. (Color online) Temperature dependence of the lattice parameters a, c of $PbTiO_3$ unit cell. The data in crossed symbols are derived from current AIMD simulations, the open symbols are from the XAFS measurements by Sicron *et al.* [12,14], and the closed symbols are from the x-ray diffraction by Shirane *et al.* [1].

by x-ray or neutron diffraction, especially at the temperatures above T_c. Compared to the conventional x-ray or neutron diffraction which provides average structural information on a length scale of millimeters and a time scale of seconds, the XAFS technique based on a synchrotron light source can probe local structure information at the atomic scale with a very short effective measuring time ($\sim 10^{-16}$ s) [12]. The length and time resolutions in the XAFS measurement are similar to those in our AIMD simulations, whereas those in conventional x-ray or neutron diffraction are too large to explore the time-dependent local distortions. As shown in Figs. 1 and 2, the large c/a ratio and the displacements of Ti atoms above T_c demonstrate that the local tetragonal distortions remain at high temperatures, indicating the presence of the order-disorder phase transition mechanism in addition to the

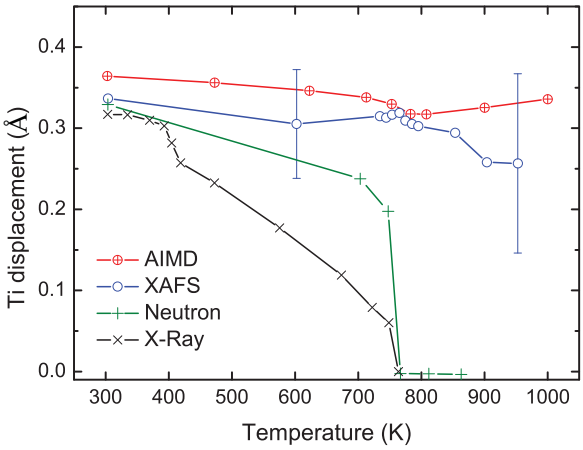

FIG. 2. (Color online) The displacement of Ti from the midpoint between the O_1 and O_3 atoms as shown in Fig. 3. The crossed circles are from current work, the open circles are from the XAFS measurements [12–14], and the "+" and "×" are the results from neutron [31] and x-ray [32,33] diffractions, respectively.

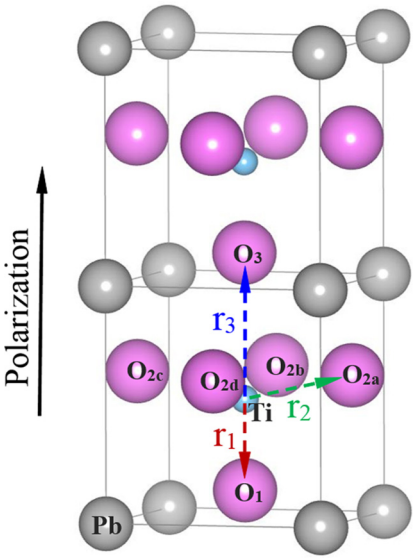

FIG. 3. (Color online) Schematic of the atomic structure of ferroelectric $PbTiO_3$ with two unit cells.

displacive mechanism. Nevertheless, in order to gain a deep insight into the evolution of local distortions and polarizations during the FE-PE phase transition, more detailed analyses are indispensable.

In ABO_3-type ferroelectric perovskites, the anisotropic distortion from the ideal cubic configuration arises from the covalent nature of B-O bonds [7,19]. For $PbTiO_3$, we thus focus on the octahedral cluster forming by a centered Ti atom and its six nearest-neighboring oxygen atoms to explore the evolution of local atomic configuration and polarization as a function of time and temperature. The schematic structure of the ferroelectric $PbTiO_3$ is illustrated in Fig. 3, where $r_{2x}(x = a, b, c, \text{or } d)$ represents the Ti-O bond length close to the (001) plan, and r_1 and r_3 the Ti-O bond lengths in the $\langle 001 \rangle$ direction. Due to their equivalency, we take r_2 as the average of r_{2a}, r_{2b}, r_{2c}, and r_{2d} in our statistical analyses. In the current study, the atomic configurations with different degrees of distortions are classified according to the relevance of the three types of bond length. If $r_1 = r_2 = r_3$, the local atomic configuration is counted as cubiclike; otherwise, it is tetragonal-like. During AIMD simulations, even for the cubic configuration at a constant temperature, the three bond lengths, r_1, r_2, and r_3, fluctuate as a function of time and are not exactly equal to each other at an instant time t . Therefore, we introduce a statistical uncertainty parameter ε to judge whether $r_1(t) = r_3(t)$ and $r_2(t) = r_3(t)$. When $|1 - \frac{r_1(t)}{r_3(t)}| \leqslant \varepsilon$, we have that $r_1(t)$ is equal to $r_3(t)$, and the same for $r_2(t)$ and $r_3(t)$. In the present work, two types of uncertainty parameters are tested: One is a temperature-independent constant of $\varepsilon = 0.10$, denoted by ε_1, and the other is based on the standard deviation of r_1/r_3 and r_2/r_3, which are temperature dependent and denoted by ε_2. It should be noted that, at a given temperature, ε_2 is specific to each Ti atom and the respective bond length ratio of r_1/r_3 or r_2/r_3. The variation range of ε_2 is shown in the Supplemental Material [27].

The fractions of local atomic environments represented with $r_1 = r_3$, $r_{2x} = r_3$ ($x = a, b, c$, or d), or $r_1 = r_2 = r_3$ based on the uncertainties of ε_1 and ε_2 are plotted in Figs. 4(a) and 4(b), respectively, obtained from a statistic of 27 Ti atoms and about 7000 AIMD configurations. Figure 4 clearly shows that both analyses predict the similar evolution trends of various local atomic environments as a function of temperature. A sudden change occurs at about 760 K, the experimentally measured FE-PE phase transition temperature. This almost exact match of the transition temperature is probably because the experimental lattice parameters are used in the simulations. By comparing the results from ε_1 and ε_2, it can be seen that the results based on ε_2 are more reasonable. Above the phase transition temperature, r_1, r_2, and r_3 should be statistically equivalent, and hence the same fractions for the local atomic configurations with $r_1 = r_3$ and $r_2 = r_3$. This feature is captured by ε_2, but not by ε_1. Therefore, our following analyses and discussions are based on the results from ε_2.

As mentioned before, for local atomic configurations with $r_1 = r_2 = r_3$, the unit cell of $PbTiO_3$ is counted as cubic; otherwise, it is counted as tetragonal. For the tetragonal case, if $r_1 \neq r_3$, the configuration is considered to be polarized in the $\langle 001 \rangle$ direction. As shown in Fig. 5, the fraction of the tetragonal configuration decreases with the increase of temperature, while the fraction of the cubic configuration

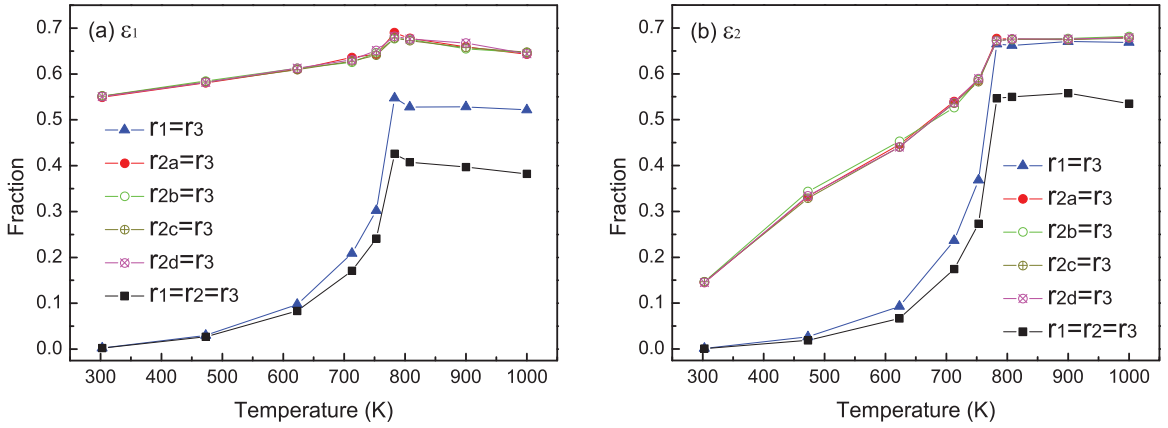

FIG. 4. (Color online) Fractions of atomic environments represented with the relevance of Ti-O bond lengths as a function of temperature based on the two considered uncertainty parameters: (a) ε_1 and (b) ε_2.

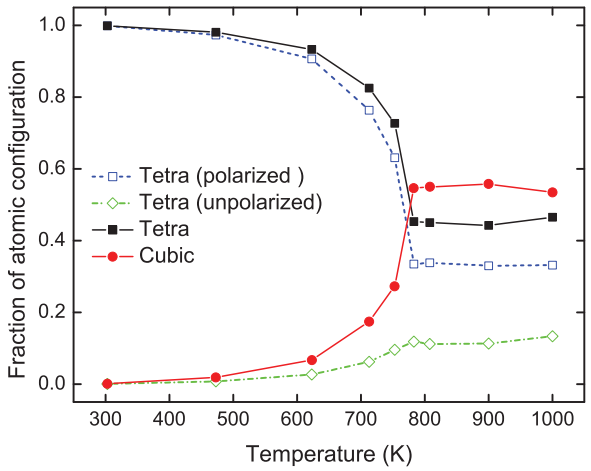

FIG. 5. (Color online) Fractions of the cubic (closed circles) and tetragonal (closed squares) configurations as a function of temperature, obtained from the AIMD simulations. Among the tetragonal configurations, the fractions of the polarized and unpolarized ones in the ⟨001⟩ direction are shown in the open squares and open diamonds, respectively.

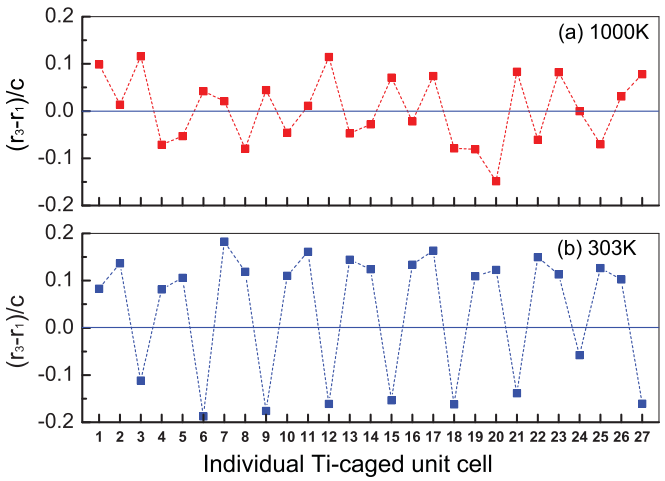

FIG. 6. (Color online) Distribution of the nominal polarizations of individual Ti-caged unit cell in the simulation supercell at (a) 1000 K and (b) 303 K at the instant of $t = 18$ ps. The positive and negative values of $(r_3 - r_1)/c$ indicate the opposite directions of local spontaneous polarization. The dashed lines are drawn for guiding eyes.

increases. Both are almost constant above the phase transition temperature. It is widely accepted in the literature [8,34] that the temperature-induced FE-PE transition in $PbTiO_3$ is first order at atmospheric pressure. Our current results show that this transition is second order, since the cubic configuration already exists at temperatures well below the phase transition temperature. The increase of the cubic configurations is continuous below T_c, and reaches a plateau once above T_c. This is consistent with our recent review on the available experimental data in the literature, concluding that the FE-PE transition in $PbTiO_3$ is second order in the pressure and temperature ranges studied under zero electric field [2]. The considerable amount of tetragonal configurations above T_c indicates the presence of the order-disorder mechanism to a large extent, in agreement with the conclusions from XAFS measurement [12–16]. Above the phase transition temperature, the tetragonal configurations could exist in different orientations, while the time- and ensemble-averaged overall structure is still cubic.

B. Local and spontaneous polarization

From Fig. 5, we can see that there are a considerable amount of tetragonal configurations with polarization above the phase transition temperature even though the whole system is in the cubic structure and does not have net polarization in any directions. The reason is that some polarized directions of the Ti-centered unit cells are opposite to each other due to the thermal fluctuations at high temperatures, resulting in the zero net polarization, as illustrated by Fig. 6. It can be seen that at 1000 K, not only the overall magnitude of the nominal polarizations [represented by $(r_3 - r_1)/c$] is smaller, but also their directions are more likely to be opposite, as compared to 303 K. Again, this result indicates the presence of a certain degree of order-disorder mechanism in the FE-PE phase transition of $PbTiO_3$, as reported in the literature [12–16].

To further investigate the details of polarization, the spontaneous polarization per unit cell can be derived as [35,36]

$$P_S = \frac{1}{V}\sum_i Z_i^* u_i, \tag{1}$$

where V denotes the volume of unit cell, Z_i^* the Born effective charge, and u_i the displacement of ion i along the ⟨001⟩ direction in the unit cell of the ferroelectric state with respect to a reference paraelectric state (see Fig. 7). In this study, the theoretical values of Born effective charge tensors by Zhong *et al.* [37] are used, and u_{Ti} and u_O at each temperature are obtained from statistical analysis of the AIMD configurations, as plotted in Fig. 7. It should be noted that although the

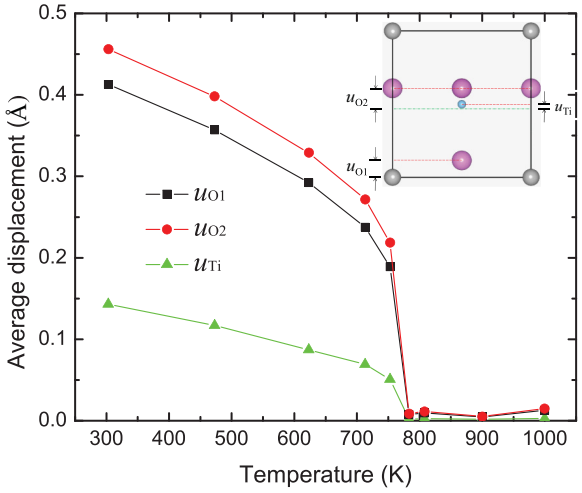

FIG. 7. (Color online) The displacements of O and Ti ions along ⟨001⟩ direction as a function of temperature. The inset illustrates the definition of displacements with respect to the centrosymmetric cubic structure.

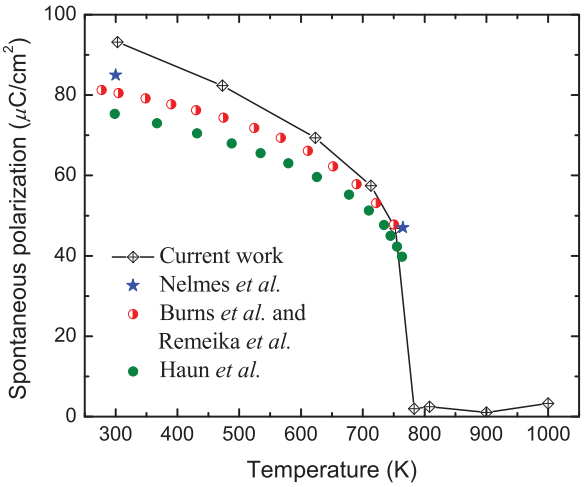

FIG. 8. (Color online) Variation of the polarization as a function of temperature, in comparison with available experimental data. The blue stars are from Ref. [38] and the green closed circles are from Ref. [39]. The red half-closed circles are quoted based on Refs. [10,40], and the polarization data were derived as $P_S = P_0 + \Delta P$, where the $P_0 = 42\,\mu$C/cm^2 at the Curie temperature [10] and ΔP were from Ref. [40].

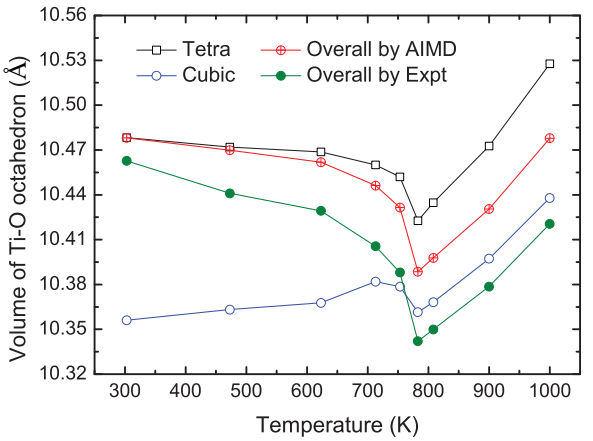

FIG. 9. (Color online) Temperature dependence of the volume of Ti-O octahedral clusters, showing the negative and positive thermal expansion. The volumes of Ti-O octahedra in the tetragonal and cubic configurations are shown in the open squares and open circles, respectively. The volumes of the overall Ti-O octahedra from current AIMD simulation and the experiment measurement by Shirane *et al.* [1] are shown in the crossed and closed circles, respectively.

experimental lattice parameters are used in our AIMD simulations, all the ionic positions are initially at the paraelectric state and allowed to displace during simulations, and therefore the ionic displacements are spontaneous in the AIMD simulations so as to reach thermodynamically more stable structures. The predicted spontaneous polarization is plotted in Fig. 8 as a function of temperature. Our predicted spontaneous polarizations at 303 and 753 K are 93.2 and 46.8 μC/cm^2, respectively, in reasonable agreement with the values of 85 and 47 uC/cm^2 by Nelmes *et al.* [38] through neutron diffraction and 81 and 42 μC/cm^2 by Burns *et al.* [10] through Raman spectroscopy. In Fig. 8, the P_S by Haun *et al.* [39] show the largest deviations compared to current predictions, which is probably because their data were indirectly calculated from the lattice strains based on the phenomenological Landau-Devonshire theory. It can be seen that with the increase of temperature, the overall spontaneous polarization decreases gradually and becomes zero at the FE-PE phase transition temperature.

IV. DISCUSSIONS

The above observations are significant in two aspects. Firstly, a considerable amount of cubic configurations already exists at 473 K, about 300 K below the transition temperature. Based on our recent work [41], this is the origin of negative thermal expansion in this system since the cubic configuration has smaller volume and higher entropy than the tetragonal configuration, resulting in a two-phase equilibrium line with a negative slope in its temperature-pressure phase diagram [2]. The higher entropy of the metastable cubic configuration reduces the free energy difference between the two configurations as the temperature increases. The thermal fluctuation of the metastable cubic configurations in the stable tetragonal matrix becomes statistically significant due to the structural configuration entropy arising from the mixture of metastable and stable configurations [42]. As shown in Fig. 9, the cubic configuration has a much smaller volume than the tetragonal configuration, while the former has a positive thermal expansion and the latter has a slight negative thermal expansion at low temperatures. The replacement of the tetragonal configuration by the cubic configuration of smaller volume significantly contributes to the thermal negative expansion of the overall system. Above the FE-PE transition, positive thermal expansion resumes because the positive thermal expansions of the two configurations become dominant.

Secondly, the amount of tetragonal configuration remains high above the FE-PE transition temperature due to its energetic favorable configuration. It is evident that the relative amounts of tetragonal and cubic configurations depend on the choice of statistical uncertainty parameter ε, but it should not change the qualitative behavior. It further supports that the FE-PE transition in $PbTiO_3$ is intrinsically second order, similar to magnetic transitions [42,43]. On the other hand, the FE-PE transition is also fundamentally different from a magnetic transition because the magnetic spin is typically kept above the magnetic transition, which primarily involves magnetic spin disordering with temperature increase, while in the present FE-PE transition, the soft-mode-driven displacive mechanism dominates in addition to a certain degree of the order-disorder mechanism.

V. SUMMARY

The evolution of atomic configurations of $PbTiO_3$ at atmospheric pressure as a function of temperature is investigated by means of AIMD simulations. The local atomic configurations and polarization are analyzed by Ti-O bond lengths as a function of time, different from conventional average over time. Our results show that both tetragonal and cubic local atomic configurations coexist below and above the FE-PE transition temperature. The fraction of tetragonal configuration

decreases and that of cubic configuration increases with the increase of temperature, indicating the FE-PE transition is intrinsically second order and depicting the origin of its negative thermal expansion phenomenon. Furthermore, the variation of spontaneous polarization with temperature is obtained, showing good agreement with experimental data and fundamental difference with respect to magnetic transition. Based on the present work, we further postulate that the nonlinear anomalies in materials originate from the statistic appearance of metastable configurations promoted by the entropy of mixing of stable and metastable configurations with their energy difference comparable with the thermal energy.

ACKNOWLEDGMENTS

This work is funded partially by the National Science Foundation (NSF) through Grant No. DMR-1006557 and Office of Naval Research (ONR) under Contract No. N0014-07-1-0638. First-principles calculations were carried out partially on the CyberStar cluster at the Pennsylvania State University funded by NSF through Grant No. OCI-0821527, partially on the resources of NERSC supported by the Office of Science of the US DOE under Contract No. DE-AC02-05CH11231, and partially on the resources of XSEDE supported by NSF under Grant No. ACI-1053575.

[1] G. Shirane and S. Hoshino, J. Phys. Soc. Jpn. **6**, 265 (1951).
[2] Z. K. Liu, Z. G. Mei, Y. Wang, and S. L. Shang, Philos. Mag. Lett. **92**, 399 (2012).
[3] Z. Wu and R. E. Cohen, Phys. Rev. Lett. **95**, 037601 (2005).
[4] M. Ahart, M. Somayazulu, R. E. Cohen, P. Ganesh, P. Dera, H.-k. Mao, R. J. Hemley, Y. Ren, P. Liermann, and Z. Wu, Nature **451**, 545 (2008).
[5] J. Chen, X. R. Xing, C. Sun, P. G. Hu, R. B. Yu, X. W. Wang, and L. H. Li, J. Am. Chem. Soc. **130**, 1144 (2008).
[6] S. G. Jabarov, D. P. Kozlenko, S. E. Kichanov, A. V. Belushkin, B. N. Savenko, R. Z. Mextieva, and C. Lathe, Phys. Solid State **53**, 2300 (2011).
[7] J. L. Zhu, H. W. Xu, J. Z. Zhang, C. Q. Jin, L. P. Wang, and Y. S. Zhao, J. Appl. Phys. **110**, 084103 (2011).
[8] A. Sani and M. Hanfland, J. Solid State Chem. **167**, 446 (2002).
[9] P.-E. Janolin, P. Bouvier, J. Kreisel, P. A. Thomas, I. A. Kornev, L. Bellaiche, W. Crichton, M. Hanfland, and B. Dkhil, Phys. Rev. Lett. **101**, 237601 (2008).
[10] G. Burns and B. A. Scott, Phys. Rev. B **7**, 3088 (1973).
[11] S. A. Mabud and A. M. Glazer, J. Appl. Crystallogr. **12**, 49 (1979).
[12] N. Sicron, B. Ravel, Y. Yacoby, E. A. Stern, F. Dogan, and J. J. Rehr, Phys. Rev. B **50**, 13168 (1994).
[13] N. Sicron, B. Ravel, Y. Yacoby, E. A. Stern, F. Dogan, and J. J. Rehr, Phys. B (Amsterdam, Neth.) **208-209**, 319 (1995).
[14] B. Ravel, N. Slcron, Y. Yacoby, E. A. Stern, F. Dogan, and J. J. Rehr, Ferroelectrics **164**, 265 (1995).
[15] T. Miyanaga, D. Diop, S. Ikeda, and H. Kon, AIP Conf. Proc. **554**, 304 (2001).
[16] K. Sato, T. Miyanaga, S. Ikeda, and D. Diop, Phys. Scr., T **115**, 359 (2005).
[17] G. Shirane, J. D. Axe, J. Harada, and J. P. Remeika, Phys. Rev. B **2**, 155 (1970).
[18] M. T. Dove, Am. Mineral. **82**, 213 (1997).
[19] R. E. Cohen, Nature **358**, 136 (1992).
[20] V. Srinivasan, R. Gebauer, R. Resta, and R. Car, AIP Conf. Proc. **677**, 168 (2003).
[21] S. C. Costa, P. S. Pizani, J. P. Rino, and D. S. Borges, J. Phys.: Condens. Matter **17**, 5771 (2005).
[22] B. K. Mani, C.-M. Chang, and I. Ponomareva, Phys. Rev. B **88**, 064306 (2013).
[23] H. Z. Fang, X. Hui, G. L. Chen, and Z. K. Liu, Appl. Phys. Lett. **94**, 091904 (2009).
[24] H. Z. Fang, W. Y. Wang, P. D. Jablonski, and Z. K. Liu, Phys. Rev. B **85**, 014207 (2012).
[25] G. Kresse and J. Furthmüller, Phys. Rev. B **54**, 11169 (1996).
[26] G. Kresse and J. Furthmüller, Comput. Mater. Sci. **6**, 15 (1996).
[27] See Supplemental Material at http://link.aps.org/supplemental/10.1103/PhysRevB.91.024104 for overall structure evolution, lattice and uncertainty parameters and fractions of cubic configuration.
[28] S. Nosé, J. Chem. Phys. **81**, 511 (1984).
[29] A. I. Akimov, G. K. Savchuk, V. A. Rubtsov, and A. K. Letko, Crystallogr. Rep. **48**, 239 (2003).
[30] Y. Kuroiwa, Y. Terado, S. J. Kim, A. Sawada, Y. Yamamura, S. Aoyagi, E. Nishibori, M. Sakata, and M. Takata, Jpn. J. Appl. Phys. **44**, 7151 (2005).
[31] R. J. Nelmes, R. O. Piltz, W. F. Kuhs, Z. Tun, and R. Restori, Ferroelectrics **108**, 165 (1990).
[32] A. M. Glazer and S. A. Mabud, Acta Crystallogr., Sect. B **34**, 1065 (1978).
[33] M. F. Kuprianov, S. M. Zaitsev, E. S. Gagarina, and E. G. Fesenko, Phase Transitions **4**, 55 (1983).
[34] G. A. Samara, Ferroelectrics **2**, 277 (1971).
[35] Z. Y. Zhu, B. Wang, H. Wang, Y. Zheng, and Q. K. Li, Solid State Electron. **50**, 1756 (2006).
[36] G. Pilania and R. Ramprasad, Phys. Rev. B **82**, 155442 (2010).,
[37] W. Zhong, R. D. King-Smith, and D. Vanderbilt, Phys. Rev. Lett. **72**, 3618 (1994).
[38] R. J. Nelmes and W. F. Kuhs, Solid State Commun. **54**, 721 (1985).
[39] M. J. Haun, E. Furman, S. J. Jang, H. A. Mckinstry, and L. E. Cross, J. Appl. Phys. **62**, 3331 (1987).
[40] J. P. Remeika and A. M. Glass, Mater. Res. Bull. **5**, 37 (1970).
[41] Z.-K. Liu, Y. Wang, and S.-L. Shang, Scr. Mater. **65**, 664 (2011).
[42] Y. Wang, S. L. Shang, H. Zhang, L.-Q. Chen, and Z.-K. Liu, Philos. Mag. Lett. **90**, 851 (2010).
[43] Y. Wang, L. G. Hector, Jr., H. Zhang, S. L. Shang, L. Q. Chen, and Z. K. Liu, Phys. Rev. B **78**, 104113 (2008).